The Apparent Critical Decay Index at the Onset of Solar Prominence Eruptions

Francesco Zuccarello, Guillaume Aulanier, Stuart Gilchrist

The Astrophysical Journal Letters, 821:L23 (6pp), 2016 April 20 doi:10.3847/2041-8205/821/2/L23

THE APPARENT CRITICAL DECAY INDEX AT THE ONSET OF SOLAR PROMINENCE ERUPTIONS

F. P. Zuccarello, G. Aulanier, and S. A. Gilchrist
LESIA, Observatoire de Paris, Psl Research University, CNRS, Sorbonne Universités, UPMC Univ. Paris 06, Univ. Paris Diderot, Sorbonne Paris Cité, 5 place Jules Janssen, F-92195 Meudon, France; Francesco.Zuccarello@obspm.fr, Guillaume.Aulanier@obspm.fr, Stuart.Gilchrist@obspm.fr
Received 2016 February 27; revised 2016 March 24; accepted 2016 April 1; published 2016 April 15

ABSTRACT

A magnetic flux rope (MFR) embedded in a line-tied external magnetic field that decreases with height as z^{-n} is unstable to perturbations if the decay index of the field n is larger than a critical value. The onset of this instability, called torus instability, is one of the main mechanisms that can initiate coronal mass ejections. Since flux ropes often possess magnetic dips that can support prominence plasma, this is also a valuable mechanism to trigger prominence eruptions. Magnetohydrodynamic (MHD) simulations of the formation and/or emergence of MFRs suggest a critical value for the onset of the instability in the range [1.4−2]. However, detailed observations of prominences suggest a value in the range [0.9−1.1]. In this Letter, by using a set of MHD simulations, we show why the large discrepancy between models and observations is only apparent. Our simulations indeed show that the critical decay index at the onset of the eruption is $n = 1.4 \pm 0.1$ when computed at the apex of the flux rope axis, while it is $n = 1.1 \pm 0.1$ when it is computed at the altitude of the topmost part of the distribution of magnetic dips. The discrepancy only arises because weakly twisted curved flux ropes do not have dips up to the altitude of their axis.

Key words: instabilities – magnetohydrodynamics (MHD) – methods: numerical – Sun: coronal mass ejections (CMEs) – Sun: filaments, prominences

1. INTRODUCTION

Prominences are magnetic structures constituted by chromospheric-like plasma that is cooler and denser than the surrounding coronal environment. In the most widespread model, solar prominences are supported by twisted magnetic field lines that globally wrap around an axial magnetic field—called magnetic flux ropes (MFR)—so that magnetic dips in their lower windings can support prominence plasma against gravity (Demoulin & Priest 1989; Aulanier & Demoulin 1998).

The equilibrium of an MFR is governed by two competing effects: the inward-directed magnetic tension of the external overlying field that embeds the flux rope, and the outward-directed magnetic pressure between the flux rope's axis and the photospheric boundary.

Ideal magnetohydrodynamic (MHD) instabilities or loss of equilibrium can lead to the rupture of this equilibrium resulting in an eruption. The first studies of the properties of this equilibrium have been performed using a current-wire treatment. In these models, the equilibrium is unstable to perturbations if the external field $B_{\rm ex}$ decreases fast enough with the height z above the photospheric boundary. The instability threshold depends on the geometry of the current wire. For a straight current wire, this occurs when the current wire (i.e., a cylindrical flux rope) reaches an altitude $z_{\rm crit}$ where the decay index of the external field $n = -d(\ln B_{\rm ex})/d(\ln z)$ becomes larger than $n_{\rm crit} \simeq 1$ (van Tend & Kuperus 1978; Filippov & Den 2001). For a thin, semi-circular current wire (i.e., a flux rope with circular axis), the critical value of the decay index for the onset of the instability is $n_{\rm crit} \simeq 1.5$ (Osovets 1961; Bateman 1978; Kliem & Török 2006; Démoulin & Aulanier 2010). The latter is referred to as "torus instability."

The role of the torus instability in flux rope eruptions has also been investigated in less-idealized configurations such as line-tied T&D (Titov & Démoulin 1999) flux ropes, dynamically formed flux ropes as well as MHD relaxations of nonlinear force-free equilibria of solar active regions (Török & Kliem 2005, 2007; Fan & Gibson 2007; Isenberg & Forbes 2007; Aulanier et al. 2010; Fan 2010; Kliem et al. 2013; Amari et al. 2014; Inoue et al. 2015). These numerical MHD simulations suggest values of the critical decay index in the range $n_{\rm crit} = 1.5 - 1.9$.

In a recent paper (Zuccarello et al. 2015, ZAG15), we modeled the evolution of an asymmetric, bipolar active region when it is driven by different classes of photospheric motions. We found a critical value of the decay index at the onset of the eruption in the range $n_{\rm crit} = 1.4 \pm 0.1$ that was not significantly affected by either the pre-eruptive photospheric evolution of the active region or by the resulting different MFRs.

From an observational point of view, Filippov & Den (2001) and Filippov & Zagnetko (2008) performed a statistical study of quiescent prominences and concluded that prominences are more prone to erupt when they approach an height where the decay index of the external field is $n \simeq 1$. Recently, McCauley et al. (2015) performed a statistical study of the kinematic of ∼100 limb prominence eruptions and found that the decay index at the onset of the fast-rise is in the range [0.7–2] with a pick at $n \simeq 1.1$. These results, that have also been confirmed using the three vantage points provided by the twin *STEREO* spacecraft (Filippov 2013), motivated the interpretation that prominence are supported by straight rather than toroidal flux ropes. In this framework, Zuccarello et al. (2014) studied the evolution of an active region filament and concluded that at the time of the eruption the filament had an height where the decay index is $n \simeq 1$. Su et al. (2015) studied the eruption of a polar crown prominence and found that at the moment of the eruption the critical decay index was $n = 1 \pm 0.2$, depending on whether the top of the prominence or the center of the cavity was used to locate the height of the erupting structure.

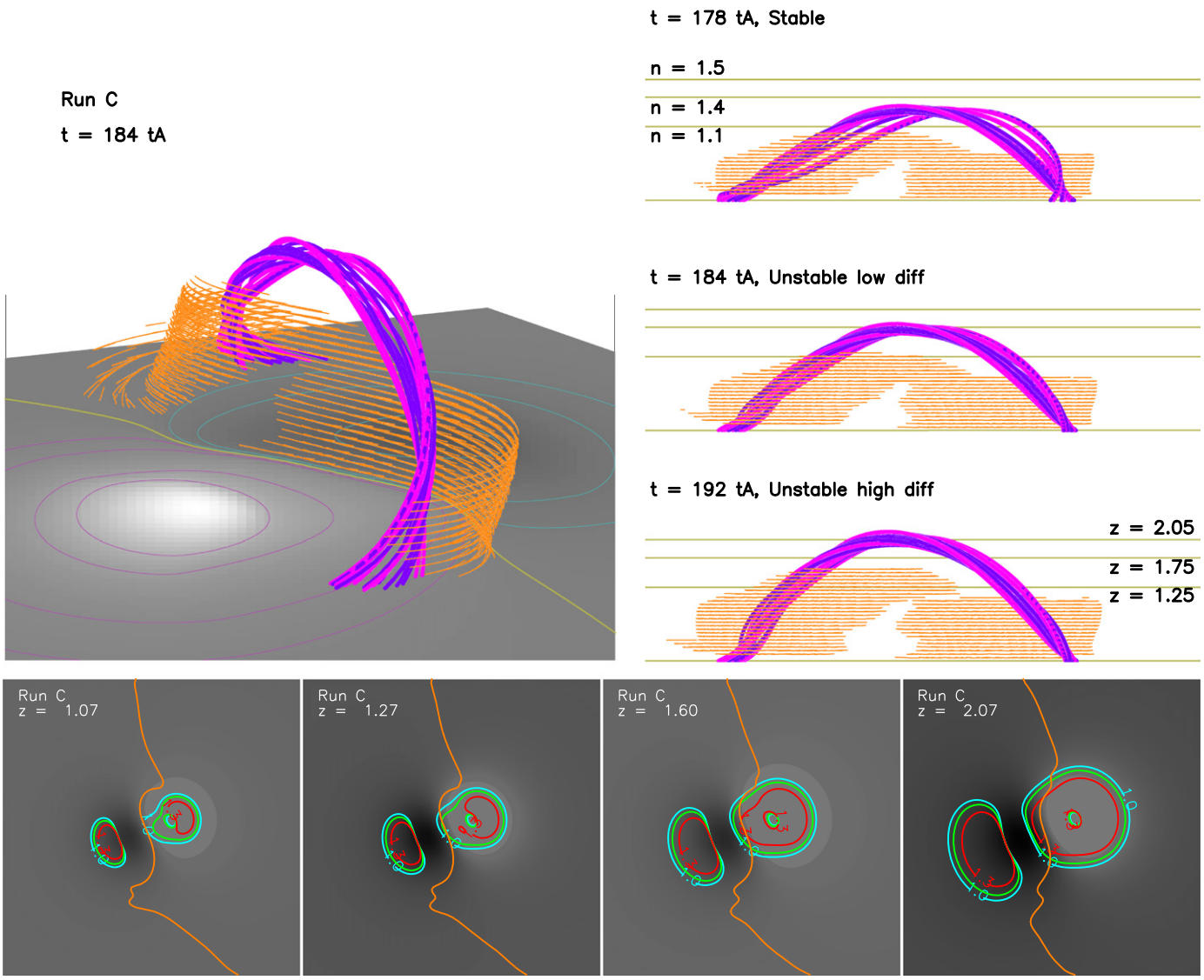

Figure 1. Top left panel: three-dimensional view of the system at the moment of the onset of the instability (under low diffusion regime) for "Run C." The dipped portion of the flux rope is highlighted by orange field lines while pink/purple field lines outline the axis of the flux rope. Right panels: side views of the system around the moment of the eruption. Horizontal lines indicate different relevant heights and critical values of the decay index for the evolution of the system (see the text for more details). Bottom row: two-dimensional maps of the decay index over plotted on B_z maps. Cyan, green, and red contours indicate decay indexes values of $n = 1$, 1.1, and $n = 1.3$. The orange contour indicates the local polarity inversion line. Left (middle-left, middle-right) panel shows the height where the PIL touches the contours $n = 1$ (1.1, 1.3). The rightmost panel shows the decay index map at the critical height for the onset of the eruption in "high diffusion" regime.

So, observational studies of prominences tend to give a lower critical value for the decay index than the MHD simulations. While these discrepancy may be due to the flux rope shapes in all the simulations, another reason may lie in the choice of where the decay index, n, is evaluated to compare to the theoretical critical value $n_{\rm crit}$. In the flux rope model paradigm, prominence observations give information only on the dipped part of the flux rope. While in cylindrical geometry magnetic dips exist up to the flux rope's axis, i.e., the location where the theoretical instability criterion is evaluated, this may not necessary be the case when curved flux ropes are considered.

In this Letter, we show that when the dipped portion of the flux rope field is taken into account in the determination of the critical decay index the discrepancy between theoretical models and observational results become less important also when quite circular MFRs are considered.

2. SIMULATED ERUPTIONS

The dynamics of the formation of MFRs is modeled by using a new hybrid MPI/OpenMP parallel version (S. A. Gilchrist et al. 2016, in preparation) of the Observationally driven High-order Magnetohydrodynamics code (Aulanier et al. 2005, 2010).

2.1. The Model

Like in ZAG15, the three-dimensional MHD equations are solved on a non-uniform mesh that expands from the center of the computational domain. As an initial condition, we consider an asymmetric active region generated by two unbalanced sub-photospheric monopoles and characterized by an initially constant Alfvén speed atmosphere, i.e., $\rho(t = 0) = B^2(t = 0)$.

The initial potential magnetic field is evolved into a current-carrying magnetic field by imposing asymmetric vortices

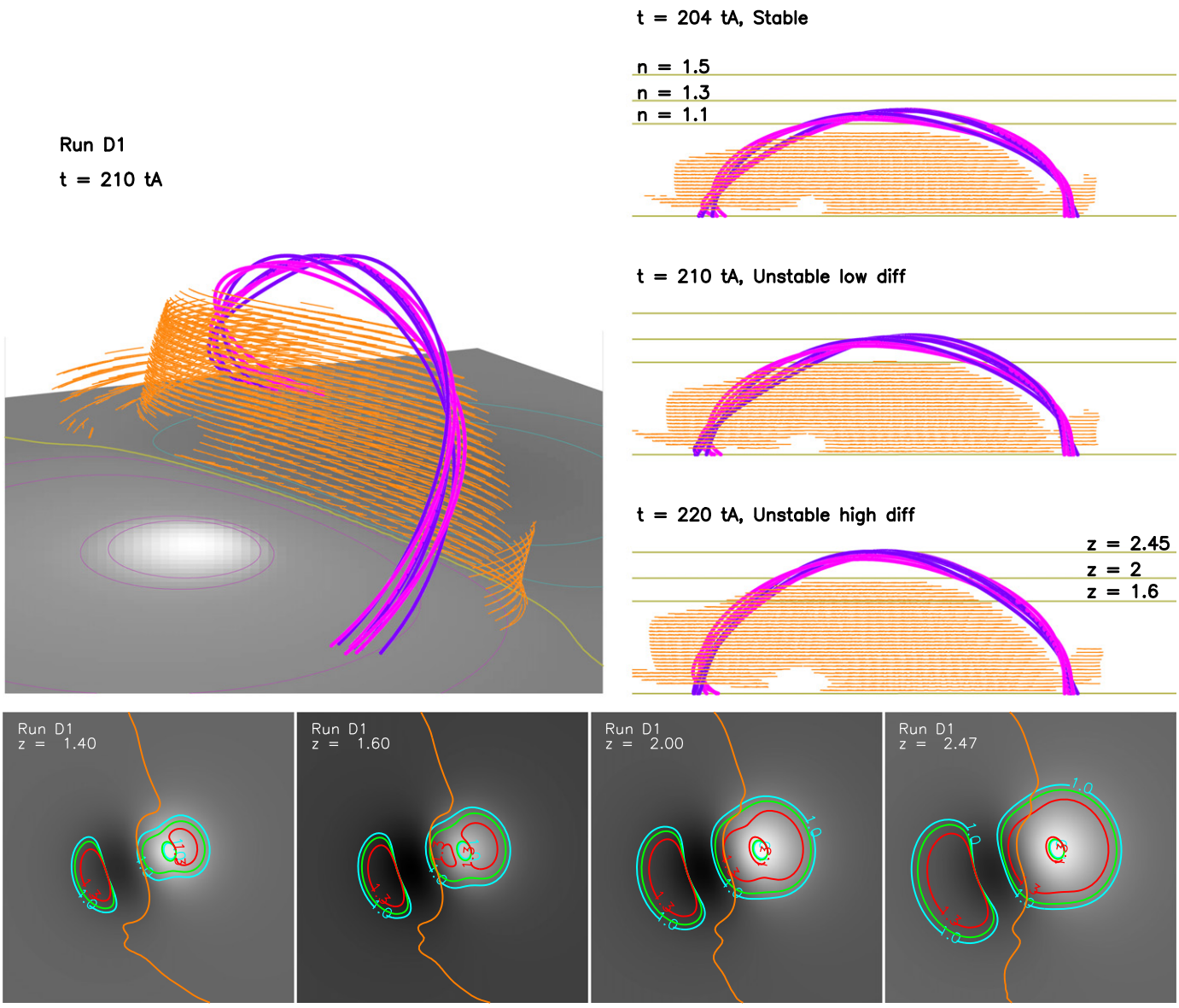

Figure 2. The same as Figure 1, but for "Run D1."

centered around the local maxima of $|B_z|$. These flows result in a magnetic field configuration charachterized by a highly sheared magnetic field close to the PIL surrounded by a quasi-potential background field anchored around the center of the magnetic polarities.

The formation and stability of MFRs is studied by applying, at the line-tied boundary, three different classes of photospheric motions. More precisely, convergence of the magnetic flux closest to the PIL ("Run C"), and peripheral and global dispersal of the magnetic field polarities (respectively "Run D1" and "D2"). The detail of the mathematical formulation of these flows is presented in ZAG15. In the latter, we also presented a fourth case, labeled as "Run S," that is not discussed in this Letter for compactness purposes.

2.2. Diffusive Coefficients and Relaxation Runs

As a result of the photospheric motions, an MFR is formed through magnetic reconnection at a bald-patch separatrix. This reconnection transfers sheared, arcade-like magnetic flux into the flux rope, eventually increasing the total current within it, and driving its slow rise up to a point when the flux rope undergoes a full eruption.

Following an approach similar to the one discussed in ZAG15, we perform relaxation runs in order to determined the critical time $t_{\rm crit}$ of the onset of the eruption. In ZAG15, we have shown that different values of the resistivity can affect $t_{\rm crit}$ and the estimation of the critical decay index $n_{\rm crit}$.

In this Letter, we focus on the trigger of the eruptions and on the value of the decay index in different key positions within and around the MFR. Therefore, all the simulations have been performed using a constant, both in space and time, coronal magnetic resistivity $\eta = 4.8 \times 10^{-4}$. At the smallest grid size, this results in a diffusive speed $u_\eta = 0.08\,\langle c_A \rangle$. In order to avoid flux to pile-up at the polarity inversion line, during the convergence phase we impose a resistivity $\eta_{\rm phot} = \eta$ also at the line-tied boundary. In what follows, this will be called the "low

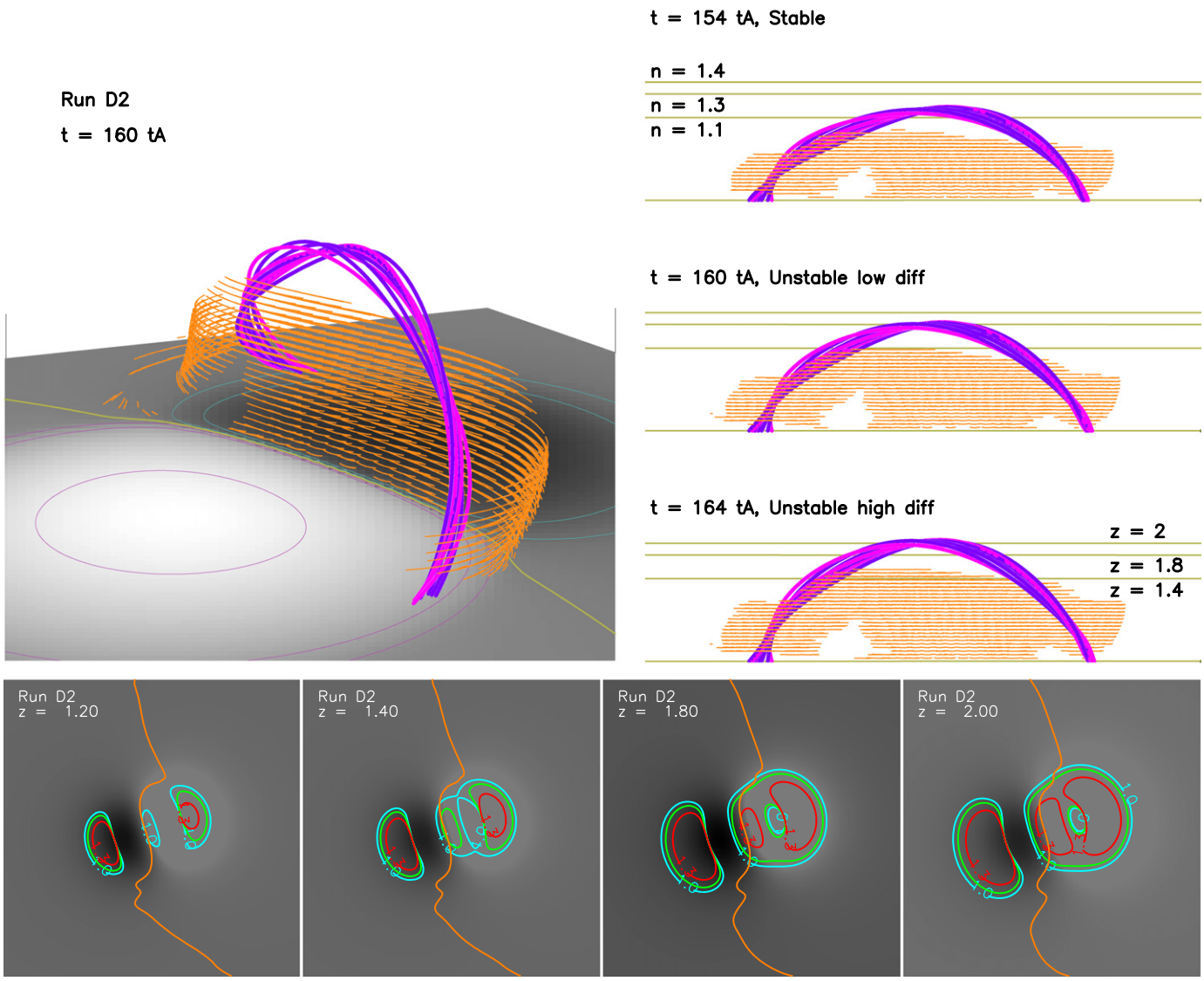

Figure 3. Same as Figure 1, but for "Run D2."

Table 1
Critical Height and Decay Index for "Low" and "High" Diffusion Simulations

Run	η ($\times 10^{-4}$)	$z_{\rm crit}$	$n_{\rm crit}$	$t_{\rm crit}/t_A$
C	4.8	1.75	1.4	184
	21	2.05	1.5	192
D1	4.8	2.00	1.3	210
	21	2.45	1.5	220
D2	4.8	1.80	1.3	160
	21	2.00	1.4	164

diffusion" regime to distinguish it from the "high diffusion" regime used during the eruption phase of ZAG15 and characterized by a resistivity $\eta = 2.1 \times 10^{-3}$.

2.3. Decay Index

To compute the decay index in our simulations, we approximate the external magnetic field, i.e., the field that is not generated by the current-carrying flux rope, with a potential (current-free) magnetic field that has the same $B_z(z = 0)$ distribution as the simulation.

In order to calculate the potential fields, we remap the output $B_z(z = 0)$ of each simulation at time $t = t_{\rm crit}$ onto a uniform grid, that is in turn inserted at the center of an eight times larger field-free grid. We then use the method of Alissandrakis (1981), and we compute the 2D maps of the decay index (see Section 3.2 of ZAG15 for more details). On the latter, the contours of the decay index for $n = 1$, 1.1, and 1.3 are plotted at different heights (see bottom rows of Figures 1–3). In these plots, the apex of the MFR lies on the portion of polarity inversion line (orange contour) that is in between the two polarities.

3. RESULTS AND DISCUSSION

The critical height ($z_{\rm crit}$) and the critical decay index ($n_{\rm crit}$) at the onset of the instability as determined through the relaxation runs under "low" and "high" coronal diffusion regimes are summarized in Table 1. The different diffusion regimes affect the critical height by about 10%–18% and the critical decay index at the flux rope's axis by about 7%–12%.

Figures 1–3 (top left panels) show the configuration of the system at the onset of the instability under "low diffusion" regime, i.e., at times $t_{crit} = 184,\ 210$, and 160 t_A, for Runs "C," "D1," and "D2," respectively.

In the figures, selected field lines are traced around the flux rope's axis (purple-pink) and in the proximity of magnetic dips (orange). The latter are locations where the magnetic field is almost horizontal and the field lines are concave-up. These are also locations where plasma can accumulate and eventually form a prominence (Aulanier & Demoulin 1998; Lionello et al. 2002; van Ballegooijen 2004; Dudík et al. 2008, 2012; Mackay & van Ballegooijen 2009; Gibson 2015). The orange magnetic field lines extend up to $z = 0.01$ above the magnetic dips. If we scale our active region to the size of a typical active region hosting quiescent prominences, i.e., about 300 Mm, then orange magnetic field lines extend up to $z \simeq 300$ km above the magnetic dips. This is comparable with the (chromospheric) pressure scale height, therefore resulting in a reasonable proxy of quiescent prominences as the ones discussed in Filippov & Den (2001).

A comparison between each simulation suggests that different photospheric motions may result in prominences with similar shapes, but different morphologies. The side views of "Run C" show that the prominence is fragmented in its central part, i.e., it has a region devoid of dips at low altitudes, and it is also asymmetric: one of its ends is higher than the other one. This is not the case for "Run D1" where the distribution of the dips seems to follow a more homogeneous circular shape. One difference between the two cases is the asymmetry of the flows that formed the flux rope: the flows in "Run C" have a higher degree of asymmetry compared with "Run D1." The details of the formation process may therefore influence the exact morphology of the flux rope and that of the dips, with these differences becoming more difficult to detect in the proximity of the flux rope's axis (ZAG15).

The right-hand side panels show the evolution of the system at three different times. The configuration in the top panels is stable, the one in the middle is unstable in the low diffusion regime, but stable in the high diffusion regime, while the configuration in the bottom panel is unstable also in the high diffusion regime. The top-two horizontal yellow lines indicate the critical decay index and critical height for the onset of the instability under "high" and "low" diffusion conditions (see Table 1), while the bottom lines in all three models indicate the height where the decay index is $n = 1.1$.

For "Run C" (respectively, "D1,""D2") at the time of the onset of the eruption in "low" diffusion regime, the apex of the axis of the MFR, i.e., the location where the stability criteria should be evaluated, has reached a height where the decay index is $n = 1.4$ (respectively, 1.35, 1.3) while the highest magnetic dips reach a height where $n = 1.1$. Interestingly, this value $n = 1.1$ is independent of the particular formation process in the three cases presented here. This suggests that the apparent instability criterion as evaluated at the location of the prominence is less sensitive to the flux rope formation process compared to when it is evaluated at the axis of the flux rope.

Similarly to the flux ropes discussed in ZAG15, these MFRs are relatively thick and have a circular axis. Therefore, the fact that a prominence (Filippov & Den 2001; Filippov & Zagnetko 2008; McCauley et al. 2015), an active region filament (Zuccarello et al. 2014), or a cavity (Su et al. 2015), becomes unstable when it reaches a critical height where $n \simeq 1$ does not necessary mean that the supporting flux rope has an elongated straight cylindrical geometry. It should be noted that our modeled prominences (within the limitations of not treating plasma thermodynamics) actually show a quite elongated straight structure that may misleadingly be interpreted as an indication that the supporting flux rope is also straight. This result suggests that the structure of the prominences is not necessarily a good tracer of the morphology and/or twist of the flux rope that supports them.

Our resulting magnetic field also shows a certain separation between the flux rope axis and top most dips as suggested by cavity observations (Hudson et al. 1999; Régnier et al. 2011; Gibson 2015; Filippov et al. 2015; Su et al. 2015; Bak-Steslicka et al. 2016). This is due to the curved geometry of the flux rope. In fact, while the height of the axis is equal to the height of the highest dips z_{dip} in a straight cylindrical flux rope, the height of the apex of the flux rope's axis can be larger than z_{dip} in a curved flux rope. The separation occurs when the radius of curvature of the dipped portion of the field lines in a straightened version of the flux rope becomes larger than the radius of curvature of the arched flux rope's axis. We find that the critical decay index computed at the flux rope's axis is $n_{crit} \simeq 1.4 \pm 0.1$, while the "apparent" critical decay index estimated by the height of the top of the prominence is $n \simeq 1.1 \pm 0.1$. Therefore, our simulations reconcile the theoretical predictions of the torus instability scenario with the previous observational results.

In conclusion, we have shown that when the appropriate location to evaluate the decay index to compare to the theoretical critical value n_{crit} is chosen, the discrepancy between theoretical predictions and observational results is significantly reduced.

The work of F.P.Z. is funded by a contract from the AXA Research Fund. F.P.Z. is a Fonds Wetenschappelijk Onderzoek (FWO) research fellow on leave. S.A.G. acknowledges the financial support of the DIM ACAV and Région Ile de France. This work was granted access to the HPC resources of MesoPSL financed by the Région Ile de France and the project Equip@Meso (reference ANR-10-EQPX-29-01) of the programme Investissements d' Avenir supervised by the Agence Nationale pour la Recherche.

REFERENCES

Alissandrakis, C. E. 1981, A&A, 100, 197
Amari, T., Canou, A., & Aly, J.-J. 2014, Natur, 514, 465
Aulanier, G., & Demoulin, P. 1998, A&A, 329, 1125
Aulanier, G., Démoulin, P., & Grappin, R. 2005, A&A, 430, 1067
Aulanier, G., Török, T., Démoulin, P., & DeLuca, E. E. 2010, ApJ, 708, 314
Bak-Steslicka, U., Gibson, S., & Chmielewska, E. 2016, FrASS, 3, 7
Bateman, G. 1978, MHD Instabilities (Cambridge, MA: MIT Press)
Démoulin, P., & Aulanier, G. 2010, ApJ, 718, 1388
Demoulin, P., & Priest, E. R. 1989, A&A, 214, 360
Dudík, J., Aulanier, G., Schmieder, B., Bommier, V., & Roudier, T. 2008, SoPh, 248, 29
Dudík, J., Aulanier, G., Schmieder, B., Zapiór, M., & Heinzel, P. 2012, ApJ, 761, 9
Fan, Y. 2010, ApJ, 719, 728
Fan, Y., & Gibson, S. E. 2007, ApJ, 668, 1232
Filippov, B. 2013, ApJ, 773, 10
Filippov, B., Martsenyuk, O., Srivastava, A. K., & Uddin, W. 2015, JApA, 36, 157
Filippov, B., & Zagnetko, A. 2008, JASTP, 70, 614
Filippov, B. P., & Den, O. G. 2001, JGR, 106, 25177

Gibson, S. 2015, in Solar Prominences, Vol. 415, ed. J.-C. Vial, & O. Engvold (Cham: Springer International), 323
Hudson, H. S., Acton, L. W., Harvey, K. L., & McKenzie, D. E. 1999, ApJL, 513, L83
Inoue, S., Hayashi, K., Magara, T., Choe, G. S., & Park, Y. D. 2015, ApJ, 803, 73
Isenberg, P. A., & Forbes, T. G. 2007, ApJ, 670, 1453
Kliem, B., Su, Y. N., van Ballegooijen, A. A., & DeLuca, E. E. 2013, ApJ, 779, 129
Kliem, B., & Török, T. 2006, PhRvL, 96, 255002
Lionello, R., Mikić, Z., Linker, J. A., & Amari, T. 2002, ApJ, 581, 718
Mackay, D. H., & van Ballegooijen, A. A. 2009, SoPh, 260, 321
McCauley, P. I., Su, Y. N., Schanche, N., et al. 2015, SoPh, 290, 1703
Osovets, S. M. 1961, in Plasma Physics and the Problem of Controlled Thermonuclear Reactions, Vol. 2, ed. M. A. Leontovich (Oxford: Pergamon), 322
Régnier, S., Walsh, R. W., & Alexander, C. E. 2011, A&A, 533, L1
Su, Y., van Ballegooijen, A., McCauley, P., et al. 2015, ApJ, 807, 144
Titov, V. S., & Démoulin, P. 1999, A&A, 351, 707
Török, T., & Kliem, B. 2005, ApJL, 630, L97
Török, T., & Kliem, B. 2007, AN, 328, 743
van Ballegooijen, A. A. 2004, ApJ, 612, 519
van Tend, W., & Kuperus, M. 1978, SoPh, 59, 115
Zuccarello, F. P., Aulanier, G., & Gilchrist, S. A. 2015, ApJ, 814, 126
Zuccarello, F. P., Seaton, D. B., Mierla, M., et al. 2014, ApJ, 785, 88